

TWENTY-ONE NEW LIGHT CURVES OF OGLE-TR-56B: NEW SYSTEM PARAMETERS AND LIMITS ON TIMING VARIATIONS¹

E. R. ADAMS^{2,3}, M. LÓPEZ-MORALES^{4,5}, J. L. ELLIOT^{3,6,7}, S. SEAGER^{3,6}, D. J. OSIP⁸, M. J. HOLMAN², J. N. WINN⁶, S. HOYER⁹, P. ROJO⁹

Draft version October 26, 2018

ABSTRACT

Although OGLE-TR-56b was the second transiting exoplanet discovered, only one light curve, observed in 2006, has been published besides the discovery data. We present twenty-one light curves of nineteen different transits observed between July 2003 and July 2009 with the Magellan Telescopes and Gemini South. The combined analysis of the new light curves confirms a slightly inflated planetary radius relative to model predictions, with $R_p = 1.378 \pm 0.090 R_J$. However, the values found for the transit duration, semimajor axis, and inclination values differ significantly from the previous result, likely due to systematic errors. The new semimajor axis and inclination, $a = 0.01942 \pm 0.00015$ AU and $i = 73.72 \pm 0.18^\circ$, are smaller than previously reported, while the total duration, $T_{14} = 7931 \pm 38$ s, is 18 minutes longer. The transit midtimes have errors from 23 s to several minutes, and no evidence is seen for transit midtime or duration variations. Similarly, no change is seen in the orbital period, implying a nominal stellar tidal decay factor of $Q_* = 10^7$, with a three-sigma lower limit of $10^{5.7}$.

Subject headings: stars: planetary systems – OGLE-TR-56

1. INTRODUCTION

OGLE-TR-56b was the second transiting exoplanet discovered, after HD209458b (Charbonneau et al. 2000; Henry et al. 2000), and the first found by a photometric wide-field survey (Udalski et al. 2002). The planetary nature of this object was confirmed by Konacki et al. (2003), who derived a mass of $1.3M_J$ from radial velocity measurements of the host star. An initial flurry of follow-up observations included radial velocity measurements by Torres et al. (2004) and Bouchy et al. (2005); the determination of the host star’s fundamental parameters and chemical composition by Santos et al. (2006); and more recently the detection of OGLE-TR-56b’s atmosphere by Sing and López-Morales (2009). However, due to the faintness of the target ($V = 16.56$, $I = 15.3$) and the recent explosion in the number of other, brighter transiting systems, OGLE-TR-56b remains relatively unstudied, despite having one of the shortest known periods (1.2 days). The radius of the planet is currently constrained by only two light curves: the composite OGLE discovery light curve in I (Udalski et al. 2002), and a

single light curve in 2006 observed alternately in Bessel R and V filters (Pont et al. 2007). The precision of the planetary parameters for this system has thus far been limited by the photometric quality of the available transit light curves (Southworth 2008) and not by the precision of the stellar parameters, as is currently the case for many other planets.

OGLE-TR-56b was selected in 2006 as part of our campaign of high-quality photometric observations to search for transit timing variations (see Adams 2010; Adams et al. 2010a,b, 2011). Its short orbital period allows for many observational opportunities, and it remains one of the better candidates to search for changes in the orbital period due to orbital decay. Predictions vary widely on the time scale over which orbital decay would be observable (Sasselov 2003; Pätzold et al. 2004; Carone and Pätzold 2007; Levrard et al. 2009), with estimates of the remaining lifetime of this system ranging from a few billion years (Sasselov 2003) to a much shorter 7 Myr (assuming $Q_* = 10^6$ Levrard et al. 2009) using very different assumptions about tidal equilibrium modes. Therefore, the estimates for the decrease in the orbital period due to orbital decay range from 0.1 to 10 ms yr^{-1} . This value is only a few times smaller than the current error on the orbital period (86 ms from Pont et al. 2007).

Here we present twenty-one new light curves of nineteen transits of OGLE-TR-56b, observed from 2003 to 2009, which we use to improve the planetary system parameters and also to search for potential timing anomalies in this system, including transit timing variations (TTVs) caused by interactions other bodies in the system, and transit duration variations (TDVs) caused by orbital precession, among other effects. In § 2 we describe the collection and analysis of the data. In § 3 we describe the transit model fitting; we note the difference in light curve shape compared to the light curve published by Pont et al. (2007) in § 3.3. In § 4 we present the revised transit ephemeris and discuss how the timing constrains the presence of other objects in the system.

¹ This paper includes data gathered with the 6.5 meter Magellan Telescopes located at Las Campanas Observatory, Chile.

² Harvard-Smithsonian Center for Astrophysics, 60 Garden St., Cambridge, MA, 02138

³ Department of Earth, Atmospheric, and Planetary Sciences, Massachusetts Institute of Technology, 77 Massachusetts Ave., Cambridge, MA, 02139

⁴ Institut de Ciències de l’Espai (CSIC-IEEC), Campus UAB, Facultat de Ciències, Torre C5, parell, 2a pl, E-08193 Bellaterra, Barcelona, Spain

⁵ Visiting Investigator; Carnegie Institution of Washington, Department of Terrestrial Magnetism, 5241 Broad Branch Road NW, Washington, DC 20015-1305

⁶ Department of Physics, Massachusetts Institute of Technology, 77 Massachusetts Ave., Cambridge, MA, 02139

⁷ Lowell Observatory, 1400 W. Mars Hill Rd., Flagstaff, AZ 86001

⁸ Las Campanas Observatory, Carnegie Observatories, Casilla 601, La Serena, Chile

⁹ Astronomy Department, Universidad de Chile, Casilla 36-D, Santiago de Chile, Chile

2. OBSERVATIONS AND DATA ANALYSIS

Nineteen transits were observed between 2003 July and 2009 July, all but one with the Magellan telescopes. All transits are referred to by the UTC date of observations; when multiple light curves exist for a given UTC date, e.g. the two light curves on 2005 April 19 UT in the Johnson *B* and *I* band, they are denoted respectively as 20050419B and 20050419I. Seven full or partial transits were observed by the Transit Light Curve (TLC) collaboration (e.g., Holman et al. 2006) during 2003-2006, using MagIC-SITe. Thirteen transits were observed between 2006-2009 on Magellan using three instruments: POETS (3 transits), IMACS (1 transit), and MagIC-e2v (9 transits). One additional transit was observed in 2009 using GMOS on Gemini South. Details on instrument setup and observational conditions are summarized in Table 1.

The Magellan instruments all had relatively small fields-of-view with high spatial sampling. The earliest transits used the Magellan Instant Camera (MagIC) with the original SITe CCD on the Clay telescope. MagIC-SITe had a field of view of $140'' \times 140''$ and a plate scale of $0.069''$ per pixel; the CCD gain was about 2 e-/ADU and the read noise 6 e- . Four filters were used: Harris *B*, Mould *I*, and Sloan *r'* and *z'* (the filter transmission curves are shown in the legend of Figure 1). In June and July 2006, POETS (Portable Occultation, Eclipse, and Transit System) was installed as a visiting PI instrument on the Clay telescope. POETS has a field of view of $23'' \times 23''$ and a plate scale of $0.046''$ per pixel. The camera is a frame-transfer CCD which can be GPS triggered and is described in Souza et al. (2006). POETS was operated full-frame (no binning) in conventional mode with a gain of 3.4 e-/ADU and read noise of 6 e- . For the first two transits observed, a Schuler Astrodon Johnson-Cousins *Is* filter was used. For the third transit, observed on 20 July 2006, coincidentally the same night as the transit by Pont et al. (2007), no filter was used as a test to achieve greater throughput; the POETS CCD is sensitive to wavelengths between 400-900 nm (Gulbis et al. 2008). We refer to this as 20060720N to distinguish it from the Pont et al. (2007) observations.

One transit was observed in 2007 with the Inamori Magellan Areal Camera and Spectrograph (IMACS) on the Magellan Baade telescope (Dressler et al. 2006). We used the $f/4$ imaging mode with a subraster on one of the eight instrument CCDs (chip 2), reading out 1200×1200 pixels centered around $x=1080$ and $y=3015$, in order to decrease the readout time to roughly 35 seconds per frame in FAST mode. The area imaged was thus $133'' \times 133''$, with a plate scale of $0.11''$ per pixel. This chip has a gain of 0.9 e-/ADU and read noise of 4.6 e- . A wideband filter, WB6300-9500, was used.

Between January 2008 and December 2009, the Magellan Instant Camera (MagIC) was mounted on the Magellan Baade telescope with the addition of a new e2v CCD. The MagIC-e2v detector, which shares a dewar with the older SITe CCD, is identical to the red CCD on HIPO (one of the first generation instruments to be flown on SOFIA), a fast read-out direct imaging camera that uses the LOIS control software (Dunham et al. 2004; Taylor et al. 2004; Osip et al. 2008). All of the MagIC-e2v transits were observed in the Sloan *i'* filter. The MagIC-e2v camera has a field of view of $38'' \times 38''$ and a plate scale

of $0.037''$ per pixel unbinned. The camera can be operated in two different modes: single exposure mode, with a readout time of about 5 seconds per exposure, which was used for the first three transits in 2008; and frame transfer mode, with a readout time of only 3 milliseconds between frames in an image cube, which was used for the following six transits. The gain and read noise of the transits observed in 2008 were 2.4 e-/ADU and 5.5 e- per pixel, respectively, and two amplifiers were used during readout; after July 2008, the CCD was reconfigured to have a gain of 0.54 e-/ADU and 5 e- read noise per pixel and a single readout amplifier.

The transits observed with the frame transfer camera POETS were observed at a very rapid cadence (2-6 s per exposure), in order to get good time sampling during transit ingress and egress. However, the noise per frame was such that we chose to bin every 10 frames (20 s) for 20060622, 8 frames (32 s) for 20060714, and 10 frames (60 s) for 20060720N. In subsequent transits, the exposure times were adjusted to maintain roughly 10^6 integrated photons for both the target and multiple nearby comparison stars. Exposure times for unbinned (1×1) data ranged from 17-60 sec, and for binned data from 10-60 sec. Details of the observing settings are noted in Table 1. Gaps in the data for transits 20060622, 20060714, and 20080727 were caused by separate instrument computer glitches, while the gap in transit 20090510 was due to observing a gamma ray burst for another project while OGLE-TR-56b passed through zenith.

The observation strategy for the transits observed by the Transit Light Curve collaboration between 2003-2006 is similar to that of OGLE-TR-111b. Details are provided in Winn et al. (2007).

The transit on 20090428 was observed using GMOS (Gemini Multi-Object Spectrograph) at Gemini South Telescope. The observations were done in service mode using a Sloan *i* filter (*i_GO327*), 2×2 binning, and an integration time between 12 and 30 seconds. We used the Region of Interest (ROI) of the camera in order to reduce the readout time to only 24 seconds in fast readout mode and low gain. 309 frames of 1024×2304 pixels were obtained with a scale of $0.146''$ per pixel. The chip has a gain of 5 e-/ADU and read noise of 7.8 e- .

Accurate timing is of the utmost importance for this project, so special care was taken to ensure that the correct times were recorded in the image headers. For the transits observed with POETS in 2006, each image frame was triggered by a GPS, so the UTC start times are accurate to the microsecond level. For the transits observed with GMOS, MagIC-SITe, IMACS and MagIC-e2v (in 2008), the UTC start times for each image were recorded from network time servers, which in most cases were verified by eye to be synchronized with the observatory's GPS clocks at the beginning of each night. For the MagIC-e2v observations in 2009, the times came from a small embedded control computer (a PC104), which received unlabeled GPS pulses every second. As with the network time servers, the PC104 was synchronized with the observatory's GPS before each transit observation. In all cases the UTC time signals written to the image headers agree within one second with the GPS time, as verified by examining the system control logs.

2.1. Data analysis

All data were calibrated using IRAF¹⁰. The zero level for POETS and IMACS data frames were calculated from bias frames taken before or after the transits, while the MagIC data frames were corrected using overscan regions on each image. The images were flat-fielded using either dome or twilight flats in the appropriate filter, as available. The GMOS data were reduced using the Gemini pipeline.

Although OGLE-TR-56 is in a very crowded field (Figure 2), the generally excellent seeing and good spatial resolution of the detectors allowed for high-quality light curves using aperture photometry. Most of the photometry was done using the IRAF routine *phot*, part of the *apphot* package. A wide range of apertures and different comparison stars were examined, depending on the nightly conditions (e.g., seeing) and specific field of view, in the same way as described for other planets we have analyzed (Adams et al. 2010a,b, 2011).

For a few transits, an alternative aperture photometry method was used to achieve greater precision. In this method, boxes were drawn around the target and comparison stars, and the sky was determined using a single 30-pixel box drawn around an empty region of sky (not easy to find for targets in crowded fields, such as OGLE-TR-56b). This method, as implemented in *Mathematica*, is both slower and not as robust as IRAF’s *phot*, particularly for data sets in which the stars shifted by more than a few pixels; but for two transits (20060622 and 20080514) it produced lower out-of-target scatter and cleaner light curves. The sky region for 20060622 was centered 2.1" west and 0.1" south of the transiting planet host star; for 20080514 the region was located 2.0" east and 0.3" south.

We additionally explored using image subtraction (Alard and Lupton 1998; Alard 2000) to create the light curve for one transit, 20090504. This test produced a light curve with slightly better scatter compared to the aperture light curve (1.0 vs 1.1 mmag in 2 min), but the depth of the image-subtracted light curve is much shallower ($k = 0.092 \pm 0.002$) than the aperture light curve for either the individual fit for that light curve ($k = 0.102 \pm 0.004$) or the joint fit ($k = 0.1039 \pm 0.0004$). This problem is a known potential pitfall for image subtraction photometry (see e.g. discussion in Gillon et al. 2007; Adams et al. 2010a). We note, however, that image subtraction does not always give erroneous depths; the TLC light curves were created with image subtraction (Winn et al. 2007), and the depths and other parameters, particularly of the full transits, agree well with light curves made with aperture photometry.

After obtaining light curves for each transit, the out-of-transit flux of each curve was examined for linear trends against several variables: airmass, seeing, telescope azimuth, (x, y) pixel location, and time since beginning of transit. These parameters were chosen because they are either directly correlated with photometric trends (e.g. seeing, airmass), or are proxies for other effects that may be harder to measure (e.g. the telescope azimuth, which is a major component in the de-rotator rates, which were

not recorded in the headers of all transit files). The data presented no significant systematics, except in three transits, for which we fit and remove linear trends for slight slopes in the flux over time (transits 20070830 and 20090504), and a slope with seeing (transit 20080727). Since these slopes were removed before the light curve parameter fitting step (see § 3), for simplicity, it is possible that covariances between those trends and the transit parameters might have a slight effect on the individual transit parameter. However, the joint fit values are unlikely to be affected since most of the transits fit had no slopes removed.

In the case of 20060720N, the light curve observed with no filter, we found that differential color extinction dominates the light curve systematics. Differential extinction, strongly correlated with airmass, is particularly troublesome, since it affects individual comparison stars differently. We therefore took a slightly different detrending approach for this dataset. The low airmass values (1.0 to 1.1) allow a linear approximation of the airmass term when detrending. In addition, we fit a separate linear slope to the ratio of the target to each comparison star, before attempting to combine them to produce the final transit light curves. Although we initially examined 13 different comparison stars over a wide range of photometric apertures, only two comparison stars could be used in the final light curve. We note that despite the relatively low scatter of the resulting light curve, there are dangers in this approach, notably in how to accurately detrend when there is little data on one side of the out-of-transit baseline to constrain the slope removed. However, given that the resulting light curve agrees well in depth and shape with the other, filtered transits, this method seems to have worked in this case. Because correcting for differential extinction in bluer wavelengths introduces many systematic complications, we do not recommend observing planetary transits without filters as a general rule; if the goal is to achieve greater throughput, a redder wide-band filter would be a better option.

The photometric parameters used to generate each light curve are shown in Table 2. Each resulting light curve is plotted in Figure 1, together with the residuals from the best model plot, with each transit binned to two minutes for comparison. The transit fluxes and times are available as an online table; an excerpt is shown in Table 3.

2.1.1. Literature light curves

The only published high-quality light curve for OGLE-TR-56b was observed on 2006 July 20 UT with the VLT in both R and V , with alternating sequences in each filter of 7-8 exposures of 15-40 s each (Pont et al. 2007). Upon refitting that light curve (provided by F. Pont 2007, personal communication), we found that the shape of the transit does not agree well with the one obtained from the new light curves, most notably in an 18-minute discrepancy in the transit duration (see § 3.3).

In an attempt to resolve this problem, we downloaded the now publicly available on the VLT archive database raw image frames and re-analyzed the data for each filter (see Figures 1 and 3). Our new light curves, based on aperture photometry, are less precise than the original image subtraction light curve: 1.0 mmag in R -band and 1.2 mmag in V -band, compared to 0.7 mmag for the orig-

¹⁰ IRAF is distributed by the National Optical Astronomy Observatories, which are operated by the Association of Universities for Research in Astronomy, Inc., under cooperative agreement with the National Science Foundation.

inal combined V/R curve. However, the aperture light curves are consistent in transit depth and duration with the 19 other light curves presented in this paper. The revised curves, referred to as 20060720R and 20060720V henceforth, are used in all subsequent analyses, except as noted for comparison with the original photometry, which we call 20060720P. We also note that the times used in the Pont et al. (2007) light curve appear to be the start time, rather than the mid-exposure time of each frame, and thus are earlier than the corresponding points in our analysis by 8–20 s; however, this slight time offset is less than the midtime error on the transit, and cannot account for the duration difference.

We did not refit the OGLE survey light curve, which is a composite of 13 full and partial transits spanning several hundred nights (Udalski et al. 2002). However, we do use the most up-to-date published midtime of that composite light curve (Torres et al. 2004) in our timing analysis, after adding 66.184 s to correct for the UTC-TT offset (§ 4).

3. TRANSIT FITTING RESULTS

3.1. Model

Our transit model fits use the algorithm of Mandel and Agol (2002) as implemented by Carter and Winn (2009), assuming white noise. We assumed that OGLE-TR-56b has zero obliquity, oblateness and orbital eccentricity. The stellar mass and radius values used to convert the model output into physical parameters were taken from Torres et al. (2008) and are listed in Table 4. We also fixed the orbital period to $P = 1.211909$ days (Pont et al. 2007), since that parameter is only used to convert a/R_* into an orbital speed, and therefore has no major effect in the other model parameters. To model the stellar limb darkening, we assumed a quadratic law with initial values for the u_1 and u_2 parameters set to the ATLAS values for the appropriate filter (Claret 2000, 2004)¹¹ In all transits we found it necessary to fix the quadratic term u_2 . In addition, we only fit for the linear term u_1 in the transits observed in the i' and I -band filters, while leaving it fixed for the transits observed in the B , r' , z' , WB -bands and with no filter because the precision of these light curves is insufficient to constrain the value of u_1 . The values for u_1 and u_2 are calculated using the *jktld* program by Southworth (2008)¹², assuming the stellar parameter values $T = 6119$ K, $\log g = 4.2$ cm/s², $[M/H] = 0$, and $V_{micro} = 2$ km/s. We fixed the coefficients for the wideband transit 20070830 to be the same as the Sloan i' filter, since the actual filter used, WB6300–9500, is centered at the same wavelength, though about twice as wide. The limb darkening parameters for the transit with no filter were derived by setting all other parameters fixed to a joint-fit value excluding this light curve, then fitting for $u_{1,none}$ and $u_{2,none}$ alone.

3.2. Light curve fits

Each light curve was fit both independently and jointly with all other light curves using a Markov chain Monte

¹¹ Initial values: $u_{1,none} = 0.19$, $u_{2,none} = 0.25$, $u_{1,B} = 0.5458$, $u_{2,B} = 0.2504$, $u_{1,r'} = 0.4089$, $u_{2,r'} = 0.2757$, $u_{1,z'} = 0.2289$, $u_{2,z'} = 0.3112$, $u_{1,I} = 0.1958$, $u_{2,I} = 0.3561$, $u_{1,i'} = u_{1,WB} = 0.2146$, $u_{2,i'} = u_{2,WB} = 0.3569$, $u_{1,V+R} = 0.3157$, $u_{2,V+R} = 0.35265$.

¹² <http://www.astro.keele.ac.uk/jkt/codes/jktld.html>

Carlo (MCMC) method, using Gibbs sampling and Metropolis-Hastings stepping (Tegmark et al. 2004; Holman et al. 2006). This method is described in greater detail in e.g. Carter et al. (2011). Three independent chains of a million links each were combined, discarding the first 50,000 links of each chain, to avoid any potential solution biases due to the initial values of the input parameters. For each fitted parameter – the radius ratio, k , inclination, i , semimajor axis ratio, a/R_* (global parameters for all transits), limb darkening coefficients u_1 and u_2 (global for each filter), and out-of-transit flux, F_{OOT} and transit midtime, T_C (specific to each transit) – we find the posterior distribution, all of which are roughly Gaussian. The median value and 68.3% confidence intervals of each parameter distribution are reported in Table 4.

To account for excess correlated noise in the light curves, we calculated the time-averaged residuals. This is done by binning the residuals for each light curve into bins from 10 to 30 minutes, the typical time scales of correlated noise (Pont et al. 2006), and then calculating how much greater the actual noise is compared to the ideal noise assuming photon statistics. The excess noise varied from 1–2.8 times the predicted noise level, and has been included in the error bars on all transit midtime and individual parameters.

As a check that there were no additional slopes in the data that could affect the photometry, we ran a test MCMC fit to 12 light curves that included a slope with respect to airmass as an additional free parameter. None of the 12 full light curves fit in this way had a significant shift in transit parameters, so we did not include airmass slopes in the rest of our analysis.

Table 4 summarizes the joint model fit values for the planet-star radius ratio, k , inclination, i , semimajor axis ratio, a/R_* , total transit duration, T_{14} , full transit duration, T_{23} , and ingress/egress duration, $T_{12} = T_{34}$. (The total transit duration is the time from first to last contact, while the full transit duration is the time when the disk of the planet is entirely overlapping the disc of the star. The ingress and egress duration are the times it takes for the transition, and are equal if the orbit is circular. See Winn (2010) for a mathematical description of the transit nomenclature.)

We also fit each light curve independently. Table 5 reports each individual parameter and error, along with the time-averaged residual factors by which those errors have been increased. To explore variations with time, the values are plotted in Figure 3, with the joint-model fit shown as a horizontal line with $1-\sigma$ errors. A few partial or noisy light curves (20050419B, 20050419I, 20060714) have been omitted from the individual results; similarly, the radius ratio for 20030730z was fixed to the joint-fit value. In general, the independent fit results are consistent with the joint fit, with the notable exception of the original photometry for 20060720P, shown as a red triangle. No significant variations are seen in any of the studied parameters over the 6-year time span of the observations.

3.3. Comparison to previous system parameters

With twenty-one new light curves, the combined fit provides a more precise determination of the system parameters, as summarized in Table 4. The errors derived

from the photometry for the radius ratio, inclination, and semi-major axis are now significantly smaller than the error in the measured stellar radius; the component of the error in the planetary radius ratio due to stellar noise is fifteen times greater than the contribution from the photometry. Any improvement in the stellar parameters will significantly improve the precision with which the radius of OGLE-TR-56b is now known.

The radius ratio remains consistent with the value reported by Pont et al. (2007), based on a single high-precision light curve. Moreover, of the nineteen light curves with independently fit radius ratio values in Table 5, none lies more than 1.3σ from the joint-fit value. Most of the new light curves have radius ratio precisions ranging from 1-4%. The lack of change in the transit depth over time indicates that either the star is less active than the few percent level, or that the pattern of star spots changes very slowly. No evidence was seen of star spot crossings.

Although our radius ratio agrees with Pont et al. (2007), the transit duration, T_{14} is significantly longer, by 18 minutes, with corresponding differences also seen in the highly-correlated inclination and semi-major axis. The duration difference can be seen by eye, as is illustrated in Figure 4 with three light curves of the same transit on 2006 July 20. The top curve in Figure 4 corresponds to the original photometry reported in Pont et al. (2007) for the observations with the VLT. The second curve shows the same Pont et al. (2007) data frames, but with new aperture photometry in the same manner as the other transits reported in this paper. The third curve shows the same transit epoch observed independently on Magellan. The solid (black) and dashed (gray) lines in each panel show, respectively, the best fit to all new light curves, and the best fit to the Pont et al. (2007) light curve alone. A fourth curve for a different transit (20080514) is shown to illustrate the good agreement between the aperture photometry light curves and the rest of the data, though not the photometry of Pont et al. (2007).

The duration of all transits, except for 20060720P, are best fit by the longer-lasting transit model (black solid line). We thus conclude that the photometry from Pont et al. (2007) most likely suffers from some unidentified noise source that shortens the apparent duration of the transit; this problem was likely exacerbated by the lack of data immediately before transit. This finding should be taken as a caution against using single-transit light curves to argue for transit duration variations due, for example, to planetary orbital precession.

The new value obtained for the semi-major axis ratio of the system, $a/R_* = 3.065 \pm 0.022$ versus the value of 3.75 ± 0.15 derived by Pont et al. (2007), means that the planet is somewhat closer to the star than previously estimated. The implications for the planetary temperature are discussed in § 3.4. The new value for the inclination, $i = 73.72 \pm 0.18$, also means that the planet is closer to a grazing orbit than previously thought ($b = 0.859 \pm 0.003$).

We also note that the revised photometry should prompt a self-consistent reanalysis of the stellar parameters, which are now mildly discrepant. OGLE-TR-56 is faint ($V = 16.56$), and the radial velocity measurements have uncertainties from $20 - 100 \text{ m s}^{-1}$ (Torres et al. 2004; Bouchy et al. 2005). Therefore the am-

plitude of the radial velocity signal, and subsequently the mass of the star, are not well constrained. Torres et al. (2008) derived a value of $M_* = 1.228 \pm 0.0078 M_\odot$, based on the stellar density derived from the photometry of Pont et al. (2007). Combined with the orbital period, $P = 1.2119819$ days, this implies a semi-major axis of $3.76_{-0.31}^{+0.35}$, inconsistent with our new result ($a/R_* = 3.065 \pm 0.022$). The new photometry suggests a lower stellar density is required, with shifts of order -1σ in mass and $+3 \sigma$ in stellar radius needed to achieve consistent values for a/R_* . A re-analysis of the radial velocity data, perhaps including new measurements, are recommended to accurately determine the stellar parameters.

3.4. Implications for the observed planetary occultation

Sing and López-Morales (2009) obtained a z' -band occultation depth for OGLE-TR-56b of $0.0363 \pm 0.0091\%$ and a brightness temperature of $T_{z'} = 2718_{-107}^{+127}$ K, using the values of the system parameters derived by Torres et al. (2008) and an effective temperature for the star of 6119 ± 62 K. Since the system parameters have changed, we refit the occultation data in the same manner described in §3.1 of Sing and López-Morales (2009), replacing the orbital period, a/R_* , the planet-to-star radius ratio, and the orbital inclination by the new values in Table 4. The new fit gives an occultation depth of 0.0374% and a central phase of $\phi = 0.4986 \pm 0.0007$. The central phase is within the errors of the previously derived value and still consistent with a circular orbit. The occultation is 0.0011% deeper than the value derived before, but both values still agree within the measured depth uncertainty. The revised brightness temperature of the planet is $T_{z'} = 2708_{-120}^{+102}$ K, also consistent with the value derived before. Therefore, the atmospheric properties of the planet derived in Sing and López-Morales (2009) remain valid, unless significantly different values for the stellar radius and temperature are found.

4. TIMING

With twenty different transit epochs of OGLE-TR-56b measured over eight years, the timing of the system can be quite well constrained. In Table 6, we present all available transit midtimes, including the OGLE survey time from Torres et al. (2004) as well as the new transits presented in this work and the re-analyzed data from Pont et al. (2007).

We calculate a new transit ephemeris using the transit times derived from the joint fit and also including the OGLE survey time (transit 20010615). Two transits observed in alternating filters (20030730 in r' and z' and 20060720 in R and V) had divergent transit midtimes when split by filter, so we fit a single combined light curve for each transit individually (see also the combined fit parameter results in Table 5). In both cases, the midtime from the combined light curve lies between the times derived from individual filter curves and is closer to the expected time of transit; this indicates the potential for timing errors if only a partial or poorly-sampled light curve is fit. (The individual filter curves for a third transit, 20050419, observed in two filters, B and I , was left alone, because both filters cover only half a transit and yield large overlapping errors; although included in

the weighted fit, this transit has minimal impact on the resulting ephemeris.)

We find the new transit ephemeris to be:

$$T_C = 2453936.60070(44)[BJD] + 1.21191096(65)N. \quad (1)$$

where T_C is the predicted central time of a transit (note that this is the same epoch as Pont et al. 2007), N is the number of periods since the reference midtime, and the values in parentheses are errors on the last digits. The residuals from this ephemeris are shown in Figure 5, with the lower panel zoomed in on the crowded region around the zero epoch. We note that the transit midtime is robustly measured for the zero epoch, with consistent timing results whether we use the original photometry (20060720P), the new photometry (20060720V+R) for the VLT light curve, or the independent time from Magellan (20060720N). The best linear fit has a reduced $\chi^2 = 2.6$, so we have scaled the errors on the parameters in Equation 1 by $\sqrt{2.6} = 1.6$. The relatively poor reduced χ^2 suggests that the errors on some transits are still underestimated; removing the most discrepant 3-4 transits from the fit results in a reduced χ^2 of just over 1. If these errors really are correct, then it is possible that the assumption of a constant ephemeris is incorrect. The most deviant points are 20060720N at transit number 0 (-3.6σ), and 20090612 at transit number 873 (-3.4σ), but there is no reason to conclude at this time that intrinsic timing variations are responsible.

4.1. Limits placed on timing variations

The error on the revised period estimate is 56 ms, with no evidence of decrease seen over the eight year time span from 2001-2009. If we fit for a linear decrease in the orbital period over time, the rate in change of the period is $\dot{P} = -2.9 \pm 17 \text{ ms yr}^{-1}$, consistent with a constant period. Based on this result, we can derive a conservative lower limit estimate for the value of the stellar tidal decay factor, Q_* . Assuming a three-sigma upper limit on the period change (5.4 ms yr^{-1}) and Equation 5 from Levrard et al. (2009), we find that the tidal decay factor for OGLE-TR-56 is no less than $Q_* = 10^{5.7}$. Furthermore, the nominal value obtained for the period change implies a $Q_* = 10^7$.

No evidence is seen of transit duration variations. The best fit to the individual transit durations listed in Table 5, using the combined light curves 20030730r+z and 20060720R+V in place of the curves separated by filter, and omitting the much-shorter duration light curve 20060720P, finds that the total transit duration has changed by $\dot{T}_{14} = -0.3 \pm 32 \text{ s yr}^{-1}$, consistent with no change. Since the planet has a large impact parameter and nearly-grazing transits, it is possible that in the future orbital precession might lead to observable changes in the planetary duration. However, no such changes have been seen to date.

We performed numerical integrations to place limits on the perturber mass for a subset of the data, using the same method for other planets described in Adams et al. (2010a,b, 2011). Using 11 transits from 2006-2009, companion mass limits were placed down to $12M_J$ in the exterior 2:1 mean motion resonance. However, we were unable to successfully run the analysis on the full set of transit times, most likely owing either to intrinsic insta-

bility in the system (meaning very few potential companions would be stable) or an error in our assumptions (that the timing residuals are intrinsically flat). Given the high reduced χ^2 value of the constant-period fit in Equation 1, it is most likely that either a few transit errors remain underestimated, or that there are timing variations that will require more data to conclusively identify and characterize.

5. CONCLUSIONS

In this work we have presented 21 new light curves of 19 transits of OGLE-TR-56b, vastly increasing the supply of high quality data on the planet. Our fitted radius value of $1.378 \pm 0.090 R_J$ is almost identical to the previously published value, and we note that the error is almost entirely supplied by error on the stellar radius; the component of uncertainty from the photometry alone is fifteen times smaller.

The values presented for the transit duration, inclination, and semi-major axis in this work are significantly different from those reported earlier, the most likely explanation being an error in the previous photometry. The new value for $a/R_* = 3.065 \pm 0.022$ places the planet slightly closer to its star than previously thought, while the inclination, $i = 73.72 \pm 0.18$ degrees, means that planet is closer to a grazing orbit ($b = 0.859 \pm 0.003$). Furthermore, the photometrically-derived values for the semi-major axis ratio are somewhat inconsistent with the current values for the stellar radius and mass; the stellar radius would need to be larger and the stellar mass smaller in order for the values to agree. New measurements and analysis of the stellar parameters are needed to resolve this inconsistency. In particular, if the stellar radius really is larger, the planetary radius value would also increase, implying that OGLE-TR-56b has an even more inflated radius than currently thought, with implications for its composition and energy budget.

The new orbital period is $P = 1.21191096 \pm 0.00000065$ days. Although there are a few points with 3-sigma residuals, there is no reason to conclude at this time that these are transit timing variations, the most likely explanation being underestimated errors. Excluding the likely erroneous low value for the previously published duration, the transit duration has remained constant during a nine year span (2001-2009), with the best fit change $\dot{T}_{14} = -0.3 \pm 32 \text{ s yr}^{-1}$. The orbital period has likewise been constant, with $\dot{P} = -2.9 \pm 17 \text{ ms yr}^{-1}$, consistent with no change. Taking the three-sigma upper limit on the period change (5.4 ms yr^{-1}) means we can place a lower limit on the stellar tidal decay factor of $Q_* = 10^{5.7}$; the nominal value implies $Q_* = 10^7$.

E.R.A. received support from NASA Origins grant NNX07AN63G. M.L.M. acknowledges support for parts of this work from NASA through Hubble Fellowship grant HF-01210.01-A/HF-51233.01 awarded by the STScI, which is operated by the AURA, Inc. for NASA, under contract NAS5-26555. This paper makes use of observations made with the European Southern Observatory telescopes and obtained from the ESO/ST-ECF Science Archive Facility. We thank Paul Schechter for observing a transit of OGLE-TR-56b as part of MIT's Magellan queue; Brian Taylor and Paul Schechter for their

tireless instrument support; and Georgi Mandushev for

assistance with image subtraction.

REFERENCES

- Adams, E. R.: 2010, *Ph.D. thesis*, MIT, Department of Earth, Atmospheric, and Planetary Sciences
- Adams, E. R., López-Morales, M., Elliot, J. L., Seager, S., and Osip, D. J.: 2010a, *ApJ* **714**, 13
- Adams, E. R., López-Morales, M., Elliot, J. L., Seager, S., and Osip, D. J.: 2010b, *ApJ* **721**, 1829
- Adams, E. R., López-Morales, M., Elliot, J. L., Seager, S., and Osip, D. J.: 2011, *ApJ* **728**, 125
- Alard, C.: 2000, *A&AS* **144**, 363
- Alard, C. and Lupton, R. H.: 1998, *ApJ* **503**, 325
- Bouchy, F., Pont, F., Melo, C., Santos, N. C., Mayor, M., Queloz, D., and Udry, S.: 2005, *A&A* **431**, 1105
- Carone, L. and Pätzold, M.: 2007, *Planet. Space Sci.* **55**, 643
- Carter, J. A., Rappaport, S., and Fabrycky, D.: 2011, *ApJ* **728**, 139
- Carter, J. A. and Winn, J. N.: 2009, *ApJ* **704**, 51
- Charbonneau, D., Brown, T. M., Latham, D. W., and Mayor, M.: 2000, *ApJ* **529**, L45
- Claret, A.: 2000, *A&A* **363**, 1081
- Claret, A.: 2004, *A&A* **428**, 1001
- Dressler, A., Hare, T., Bigelow, B. C., and Osip, D. J.: 2006, in *Society of Photo-Optical Instrumentation Engineers (SPIE) Conference Series*, Vol. 6269 of *Society of Photo-Optical Instrumentation Engineers (SPIE) Conference Series*
- Dunham, E. W., Elliot, J. L., Bida, T. A., and Taylor, B. W.: 2004, in A. F. M. Moorwood & M. Iye (ed.), *Society of Photo-Optical Instrumentation Engineers (SPIE) Conference Series*, Vol. 5492 of *Presented at the Society of Photo-Optical Instrumentation Engineers (SPIE) Conference*, pp 592–603
- Gillon, M., Pont, F., Moutou, C., Santos, N. C., Bouchy, F., Hartman, J. D., Mayor, M., Melo, C., Queloz, D., Udry, S., and Magain, P.: 2007, *A&A* **466**, 743
- Gulbis, A. A. S., Elliot, J. L., Person, M. J., Babcock, B. A., Pasachoff, J. M., Souza, S. P., and Zuluaga, C. A.: 2008, in D. Phelan, O. Ryan, & A. Shearer (ed.), *High Time Resolution Astrophysics: The Universe at Sub-Second Timescales*, Vol. 984 of *American Institute of Physics Conference Series*, pp 91–100
- Henry, G. W., Marcy, G. W., Butler, R. P., and Vogt, S. S.: 2000, *ApJ* **529**, L41
- Holman, M. J., Winn, J. N., Latham, D. W., O’Donovan, F. T., Charbonneau, D., Bakos, G. A., Esquerdo, G. A., Hergenrother, C., Everett, M. E., and Pál, A.: 2006, *ApJ* **652**, 1715
- Konacki, M., Torres, G., Jha, S., and Sasselov, D. D.: 2003, *Nature* **421**, 507
- Levrard, B., Winisdoerffer, C., and Chabrier, G.: 2009, *ApJ* **692**, L9
- Mandel, K. and Agol, E.: 2002, *ApJ* **580**, L171
- Osip, D. J., Floyd, D., and Covarrubias, R.: 2008, in *Society of Photo-Optical Instrumentation Engineers (SPIE) Conference Series*, Vol. 7014 of *Presented at the Society of Photo-Optical Instrumentation Engineers (SPIE) Conference*, p. 9
- Pätzold, M., Carone, L., and Rauer, H.: 2004, *A&A* **427**, 1075
- Pont, F., Moutou, C., Gillon, M., Udalski, A., Bouchy, F., Fernandes, J. M., Gieren, W., Mayor, M., Mazeh, T., Minniti, D., Melo, C., Naef, D., Pietrzynski, G., Queloz, D., Ruiz, M. T., Santos, N. C., and Udry, S.: 2007, *A&A* **465**, 1069
- Pont, F., Zucker, S., and Queloz, D.: 2006, *MNRAS* **373**, 231
- Santos, N. C., Ecuivillon, A., Israelian, G., Mayor, M., Melo, C., Queloz, D., Udry, S., Ribeiro, J. P., and Jorge, S.: 2006, *A&A* **458**, 997
- Sasselov, D. D.: 2003, *ApJ* **596**, 1327
- Sing, D. K. and López-Morales, M.: 2009, *A&A* **493**, L31
- Southworth, J.: 2008, *MNRAS* **386**, 1644
- Souza, S. P., Babcock, B. A., Pasachoff, J. M., Gulbis, A. A. S., Elliot, J. L., Person, M. J., and Gangestad, J. W.: 2006, *PASP* **118**, 1550
- Taylor, B. W., Dunham, E. W., and Elliot, J. L.: 2004, in H. Lewis & G. Raffi (ed.), *Society of Photo-Optical Instrumentation Engineers (SPIE) Conference Series*, Vol. 5496 of *Presented at the Society of Photo-Optical Instrumentation Engineers (SPIE) Conference*, pp 446–454
- Tegmark, M., Strauss, M. A., Blanton, M. R., Abazajian, K., Dodelson, S., Sandvik, H., Wang, X., Weinberg, D. H., Zehavi, I., Bahcall, N. A., Hoyle, F., Schlegel, D., Scocimarro, R., Vogeley, M. S., Berlind, A., Budavari, T., Connolly, A., Eisenstein, D. J., Finkbeiner, D., Frieman, J. A., Gunn, J. E., Hui, L., Jain, B., Johnston, D., Kent, S., Lin, H., Nakajima, R., Nichol, R. C., Ostriker, J. P., Pope, A., Scranton, R., Seljak, U., Sheth, R. K., Stebbins, A., Szalay, A. S., Szapudi, I., Xu, Y., Annis, J., Brinkmann, J., Burles, S., Castander, F. J., Csabai, I., Loveday, J., Doi, M., Fukugita, M., Gillespie, B., Hennessy, G., Hogg, D. W., Ivezić, Ž., Knapp, G. R., Lamb, D. Q., Lee, B. C., Lupton, R. H., McKay, T. A., Kunszt, P., Munn, J. A., O’Connell, L., Peoples, J., Pier, J. R., Richmond, M., Rockosi, C., Schneider, D. P., Stoughton, C., Tucker, D. L., vanden Berk, D. E., Yanny, B., and York, D. G.: 2004, *Phys. Rev. D* **69(10)**, 103501
- Torres, G., Konacki, M., Sasselov, D. D., and Jha, S.: 2004, *ApJ* **609**, 1071
- Torres, G., Winn, J. N., and Holman, M. J.: 2008, *ApJ* **677**, 1324
- Udalski, A., Zebur, K., Szymanski, M., Kubiak, M., Soszynski, I., Szewczyk, O., Wyrzykowski, L., and Pietrzynski, G.: 2002, *Acta Astronomica* **52**, 115
- Winn, J. N.: 2010, *Exoplanet Transits and Occultations*, pp 55–77
- Winn, J. N., Holman, M. J., and Fuentes, C. I.: 2007, *AJ* **133**, 11

TABLE 1
OBSERVATIONAL DETAILS FOR TWENTY-ONE NEW LIGHT CURVES OF OGLE-TR-56B

Transit (UT)	Instrument	Frames ^a	Exposure (sec)	Filter	Binning	Read (sec)	Airmass	Time observed (before ingress)	Atm. stability	Seeing (arcsec)
20030730r	MagIC-SITe	47 (0)	–	r'	1x1	23	1.1–1.7	2.4 hrs (+27 min)	–	–
20030730z	MagIC-SITe	48 (0)	–	z'	1x1	23	1.1–1.7	2.4 hrs (+22 min)	–	–
20050419B	MagIC-SITe	59 (0)	–	B	1x1	23	1.0–1.6	3.2 hrs (–54 min)	–	–
20050419I	MagIC-SITe	59 (0)	–	I	1x1	23	1.0–1.6	3.3 hrs (–53 min)	–	–
20050730	MagIC-SITe	140 (0)	–	I	1x1	23	1.0–1.4	3.2 hrs (+10 min)	–	–
20050731	MagIC-SITe	113 (0)	–	I	1x1	23	1.1–1.9	3.0 hrs (+37 min)	–	–
20060622	POETS	6642 (121) ^b	2	Is	1x1	^c	1.0–1.4	3.9 hrs (+13 min)	Stable	0.25–0.5
20060626	MagIC-SITe	245 (0)	–	I	1x1	23	1.0–2.3	4.6 hrs (+71 min)	–	–
20060714	POETS	2200 (588) ^d	4	Is	1x1	^c	1.0–1.4	4.6 hrs (+88 min)	Variable	0.25–0.5
20060720N	POETS	1867 (1379) ^e	6	None	1x1	^c	1.0–1.1	5.5 hrs (+17 min)	Stable	0.4
20070830	IMACS	352 (1) ^f	15, 30	WB ^g	1x1	25	1.0–1.5	4.4 hrs (+112 min)	Stable	0.6
20080514	MagIC-e2v	187 (0)	60	i'	1x1	5	1.0–1.5	3.6 hrs (+56 min)	Superb	0.3–0.4
20080612	MagIC-e2v	604 (64) ^h	17, 20	i'	1x1	5	1.0–1.2	7.9 hrs (+264 min)	Stable	0.3–0.5
20080727	MagIC-e2v	672 (0) ⁱ	10, 12	i'	2x2	5	1.0–1.3	4.3 hrs (+100 min)	Stable	0.7
20090428	GMOS	309 (0)	12–30	i'	2x2	24	1.0–1.5	3.4 hrs (+32 min)	Stable	0.4–0.6
20090504	MagIC-e2v	623 (2) ⁱ	23, 25	i'	2x2	^c	1.0–1.2	5.5 hrs (+90 min)	Variable	0.5–1.0
20090510	MagIC-e2v	460 (2) ^f	20, 30	i'	2x2	^c	1.0–1.2	3.7 hrs (+94 min)	Stable	0.7
20090521	MagIC-e2v	626 (0)	22–25	i'	2x2	^c	1.0–1.2	4.6 hrs (+65 min)	Variable	0.4–0.7
20090612	MagIC-e2v	772 (3) ^f	17, 20	i'	2x2	^c	1.0–2.3	4.3 hrs (+63 min)	Stable	0.4–0.7
20090613	MagIC-e2v	715 (0)	20	i'	2x2	^c	1.0–2.0	4.3 hrs (+48 min)	Variable	0.6–0.8
20090728	MagIC-e2v	535 (5) ^f	30–60	i'	2x2	^c	1.0–1.2	5.3 hrs (+187 min)	Variable	0.4–0.9

^a Number of frames used (additional frames that were discarded).

^b Discarded during meridian crossing (images elongated).

^c Readout is a few milliseconds in frame transfer mode.

^d Discarded baseline after transit at a different pointing, which did not return to the same ratio level as before.

^e Discarded 31 frames during meridian crossing, 1347 frames at airmass > 1.1, and 1 frame with an aberrant ratio.

^f Discarded a few anomalous frames, e.g. due to a seeing spike on one or more frames

^g WB6300–9500, a wide band filter from 630–950 nm.

^h Discarded initial frames with low counts on target (50 points) and a minor seeing spike (14 points).

ⁱ Discarded frames with large target diameters (poor seeing): >11.5 pixel (20080727) and >11.0 pixel (20090504)

TABLE 2
APERTURE PHOTOMETRY PARAMETERS FOR EACH TRANSIT

Transit (UT)	Comp. Stars	Aperture ^a (pixels)	Sky radius, width (pixels)	Slope removed	Scatter ^b (mmag)
20060622	5	10 ^c	–	–	1.0
20060714	2	8.2	30, 10	–	1.7
20060720R	6	6.0	50, 5	–	1.0
20060720V	5	7.0	40, 5	–	1.2
20060720N	2	14	70, 5	–3.6%, –9.6% ^d	0.7
20070830	3	7.6	20, 20	–0.96% ^e	1.1
20080514	5	14.5 ^c	–	–	0.6
20080612	5	12.2	50, 10	–	0.9
20080727	3	9.0	25, 30	+0.16% ^f	1.3
20090428	4	4.0	30, 5	–	1.0
20090504	2	8.2	20, 30	+1.48% ^e	1.1
20090510	3	7.8	40, 10	–	1.0
20090521	5	7.0	30, 10	–	0.9
20090612	5	8.2	30, 10	–	0.8
20090613	3	10.2	25, 10	–	1.1
20090728	2	8.2	15, 20	–	1.2

^a Except as noted, the aperture is a circular radius around the star.

^b Scatter on out-of-transit flux, binned to 2 minutes.

^c Box half-width for alternate photometry method described in § 2.1

^d Trend removed for each star, individually, against airmass, in units of $Z \text{ day}^{-1}$.

^e Trend removed against time, in units of flux day^{-1} .

^f Trend removed against seeing in pixels, in units of flux pixels^{-1} .

TABLE 3
FLUX VALUES FOR NEW TRANSITS OF OGLE-TR-56B^a

Mid-exposure (JD_{UTC})	Mid-exposure (BJD_{TDB})	Flux	Error
2453908.670845	2453908.677416	1.002203	0.001641
2453908.670868	2453908.677439	1.007551	0.001641
2453908.670891	2453908.677462	0.9947374	0.001641
2453908.670914	2453908.677485	1.003771	0.001641
2453908.670937	2453908.677508	0.9926688	0.001641
...			

^a Full table available online.

TABLE 4
NEW SYSTEM PARAMETERS FOR OGLE-TR-56

Parameter	Value ^a
Radius ratio, k	0.1039 ± 0.0004
Semimajor axis ratio, a/R_*	3.065 ± 0.022
Inclination, i (deg)	73.72 ± 0.18
Eccentricity, e	0 (fixed)
Linear limb-darkening coefficient, $u_{1,i'}$	0.169 ± 0.033
Quadratic limb-darkening coefficient, $u_{1,I}$	0.175 ± 0.041
Impact parameter, b	0.859 ± 0.003
Total transit duration, T_{14} (sec)	7931 ± 38
Duration of full transit, T_{23} (sec)	2896^{+106}_{-100}
Ingress/egress duration, $T_{12} = T_{34}$ (sec)	2518^{+59}_{-62}
Orbital period, P (days)	$1.21191096 \pm 0.00000065$
Reference epoch, T_0 (BJD_{TDB})	$2453936.60070 \pm 0.00044$
Semimajor axis, a (AU)	0.01942 ± 0.00015^b
Planetary radius, R_p (R_J)	1.378 ± 0.090^b
Planetary mass, M_p (M_J)	1.39 ± 0.18^b
Stellar radius, R_* (R_\odot)	1.363 ± 0.089^b
Stellar mass, M_* (M_\odot)	1.228 ± 0.078^b

^a Median value of parameter distribution from joint fit to 23 light curves, with errors reported from the 68.3% credible interval.

^b Stellar mass and radius values from Torres et al. (2008).

TABLE 5
PARAMETERS FOR INDEPENDENT FITS TO EACH TRANSIT OF OGLE-TR-56B

Transit	TAR ^a	k	i (deg)	a/R_*	T_{14}	T_{23}	$T_{12} = T_{34}$
20030730r	1.7	0.10414 ± 0.0072	72.43 ± 2.8	2.836 ± 0.32	8688.0 ± 696.0	3292.1 ± 1271.0	2693.0 ± 895.0
20030730z	1.0	0.1039 (fixed)	74.05 ± 1.2	3.135 ± 0.17	7707.3 ± 298.0	2737.2 ± 637.0	2489.3 ± 372.0
20050730r+z ^b	1.6	0.09856 ± 0.004	74.47 ± 1.9	3.199 ± 0.28	7500.7 ± 417.0	3044.2 ± 836.0	2229.3 ± 558.0
20050731	1.3	0.10653 ± 0.0091	74.21 ± 1.7	3.156 ± 0.21	7728.1 ± 330.0	2749.0 ± 804.0	2485.9 ± 499.0
20060622	1.9	0.10392 ± 0.0023	74.15 ± 1.1	3.077 ± 0.14	8143.4 ± 216.0	3510.9 ± 516.0	2317.3 ± 334.0
20060626	2.1	0.09986 ± 0.0064	74.12 ± 3.9	3.095 ± 0.54	7938.0 ± 696.0	3446.9 ± 1528.0	2250.2 ± 1046.0
20060720P ^c	1.0	0.10269 ± 0.0017	77.48 ± 0.8	3.754 ± 0.15	6817.9 ± 129.0	3452.3 ± 281.0	1684.0 ± 192.0
20060720R	1.1	0.10064 ± 0.0097	73.85 ± 1.9	3.094 ± 0.24	7764.9 ± 361.0	3001.0 ± 783.0	2362.6 ± 492.0
20060720V	1.1	0.1011 ± 0.0066	76.74 ± 4.0	3.503 ± 0.7	7428.3 ± 475.0	3973.5 ± 948.0	1733.8 ± 664.0
20060720V+R ^d	1.3	0.1039 (fixed)	73.82 ± 0.9	3.092 ± 0.14	7822.6 ± 265.0	2766.6 ± 449.0	2528.1 ± 283.0
20060720N	1.6	0.1033 ± 0.0021	74.12 ± 1.1	3.116 ± 0.15	7858.5 ± 204.0	3088.4 ± 604.0	2385.5 ± 380.0
20070830	1.0	0.10228 ± 0.0018	73.91 ± 0.9	3.065 ± 0.11	8025.8 ± 182.0	3290.0 ± 439.0	2369.0 ± 283.0
20080514	1.1	0.10408 ± 0.0012	74.17 ± 0.5	3.131 ± 0.07	7817.2 ± 121.0	3008.5 ± 276.0	2405.0 ± 180.0
20080612	1.8	0.10419 ± 0.0029	73.66 ± 1.4	3.061 ± 0.18	7924.2 ± 293.0	2807.6 ± 857.0	2556.6 ± 517.0
20080727	1.7	0.10695 ± 0.0045	73.84 ± 1.6	3.08 ± 0.2	7968.5 ± 346.0	2831.0 ± 961.0	2563.7 ± 576.0
20090428	1.7	0.10751 ± 0.0108	72.74 ± 1.6	2.987 ± 0.17	7829.0 ± 296.0	1676.7 ± 935.0	3051.5 ± 528.0
20090504	2.6	0.10244 ± 0.0042	75.23 ± 2.3	3.243 ± 0.33	7817.5 ± 404.0	3712.0 ± 905.0	2053.5 ± 605.0
20090510	2.0	0.10861 ± 0.0037	73.46 ± 1.5	3.013 ± 0.19	8182.1 ± 340.0	2795.2 ± 1012.0	2691.6 ± 630.0
20090521	1.3	0.10159 ± 0.0018	74.01 ± 0.8	3.085 ± 0.1	7954.7 ± 171.0	3286.5 ± 391.0	2335.0 ± 253.0
20090612	1.9	0.10597 ± 0.0025	73.88 ± 1.1	3.07 ± 0.15	8039.0 ± 245.0	3048.9 ± 598.0	2496.1 ± 387.0
20090613	1.9	0.10429 ± 0.0039	74.67 ± 2.2	3.188 ± 0.32	7801.5 ± 433.0	3291.9 ± 926.0	2258.6 ± 641.0
20090728	2.1	0.09963 ± 0.0039	75.09 ± 2.2	3.271 ± 0.33	7524.5 ± 408.0	3377.5 ± 857.0	2076.4 ± 585.0

^a Multiplicative factor indicating excess noise, as derived from the time-averaged residual method.

^b Combined r' and z' photometry.

^c New fit to original photometry of Pont et al. (2007)

^d Combined V and R photometry.

TABLE 6
OGLE-TR-56B TRANSIT MIDTIMES AND RESIDUALS

Transit	Number	Midtime (BJD_{TDB})	O-C (s)	σ	Source
20010615 ^a	-1536	2452075.10534 \pm 0.00170	-11 \pm 147	-0.1	Torres et al. (2004)
20030730r	-896	2452850.73111 \pm 0.00092	226 \pm 80	2.9	this work
20030730z	-896	2452850.72730 \pm 0.00083	-103 \pm 72	-1.4	this work
20030730r+z ^b	-896	2452850.72908 \pm 0.00045	51 \pm 39	1.4	this work
20050419B	-377	2453479.71055 \pm 0.00540	24 \pm 466	0.1	this work
20050419I	-377	2453479.70867 \pm 0.00290	-139 \pm 246	-0.6	this work
20050730	-293	2453581.51076 \pm 0.00096	-3 \pm 83	-0.0	this work
20050731	-292	2453582.72328 \pm 0.00073	49 \pm 63	0.8	this work
20060622	-23	2453908.72603 \pm 0.00060	-63 \pm 51	-1.2	this work
20060626	-19	2453913.57171 \pm 0.00130	-233 \pm 114	-2.0	this work
20060714	-5	2453930.54256 \pm 0.00170	121 \pm 148	0.8	this work
20060720P ^c	0	2453936.59875 \pm 0.00100	-169 \pm 86	-1.9	Pont et al. (2007)
20060720V	0	2453936.59735 \pm 0.00080	-291 \pm 69	-4.2	this work
20060720R	0	2453936.60226 \pm 0.00072	134 \pm 62	2.2	this work
20060720V+R ^d	0	2453936.59973 \pm 0.00092	-85 \pm 79	-1.1	this work
20060720N	0	2453936.59908 \pm 0.00045	-141 \pm 39	-3.6	this work
20070830	335	2454342.59179 \pm 0.00046	78 \pm 40	2.0	this work
20080514	548	2454600.72852 \pm 0.00031	52 \pm 27	1.9	this work
20080612	572	2454629.81483 \pm 0.00083	90 \pm 71	1.3	this work
20080727	609	2454674.65443 \pm 0.00085	-5 \pm 73	-0.1	this work
20090428	836	2454949.75803 \pm 0.00065	-21 \pm 56	-0.4	this work
20090504	841	2454955.81712 \pm 0.00110	-61 \pm 92	-0.7	this work
20090510	846	2454961.87779 \pm 0.00069	35 \pm 60	0.6	this work
20090521	855	2454972.78553 \pm 0.00044	81 \pm 38	2.2	this work
20090612	873	2454994.59691 \pm 0.00060	-179 \pm 52	-3.4	this work
20090613	874	2454995.80961 \pm 0.00079	-111 \pm 68	-1.6	this work
20090728	911	2455040.65158 \pm 0.00093	-1 \pm 80	-0.0	this work

^a Time has been adjusted from the published times into the BJD_{TT} time system by adding UTC-TT conversion of 64.184 sec.

^b Midtime value when the r' and z' light curves are combined and fit independently.

^c Light curve from Pont et al. (2007); the midtime reported is from our independent fit of the original photometry.

^d Midtime value when the R and V light curves are combined and fit independently.

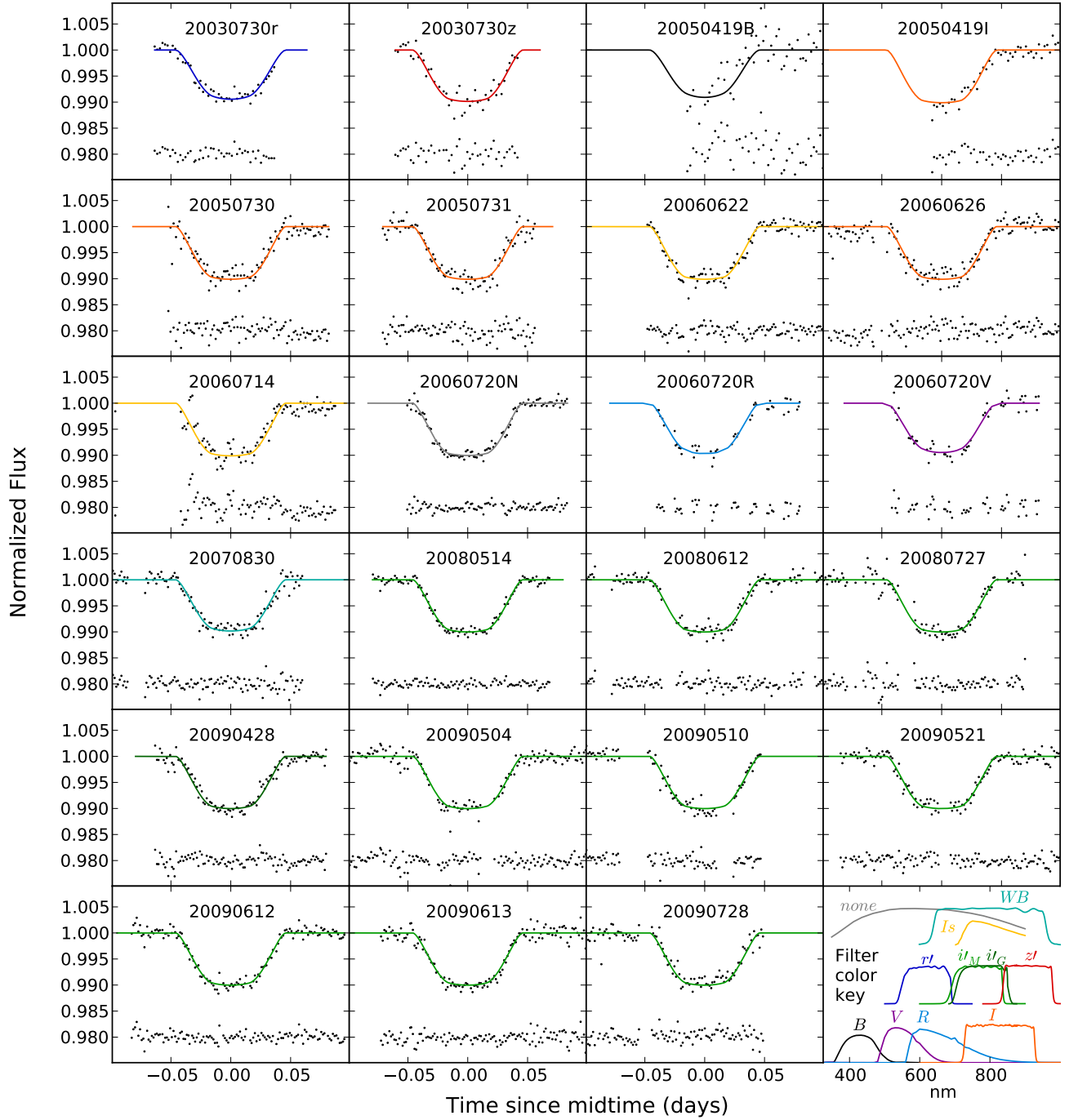


FIG. 1.— Twenty-three light curves observed over nineteen different transit epochs of OGLE-TR-56b. All data are binned to 2 minutes to aid comparison. The solid lines show the best model for all curves, color-coded by the instrument and filter used: SItE/*B* = black, FORS1/*V* = purple, SItE/*r'* = dark blue, FORS1/*R* = light blue, IMACS/*WB*6500-9300 = cyan, e2v/*i'* = green, GMOS/*i'* = dark green, POETS/*Is* = yellow, SItE/*I* = orange, SItE/*z'* = red, and POETS/no filter = gray. The residuals from the model are plotted below each curve.

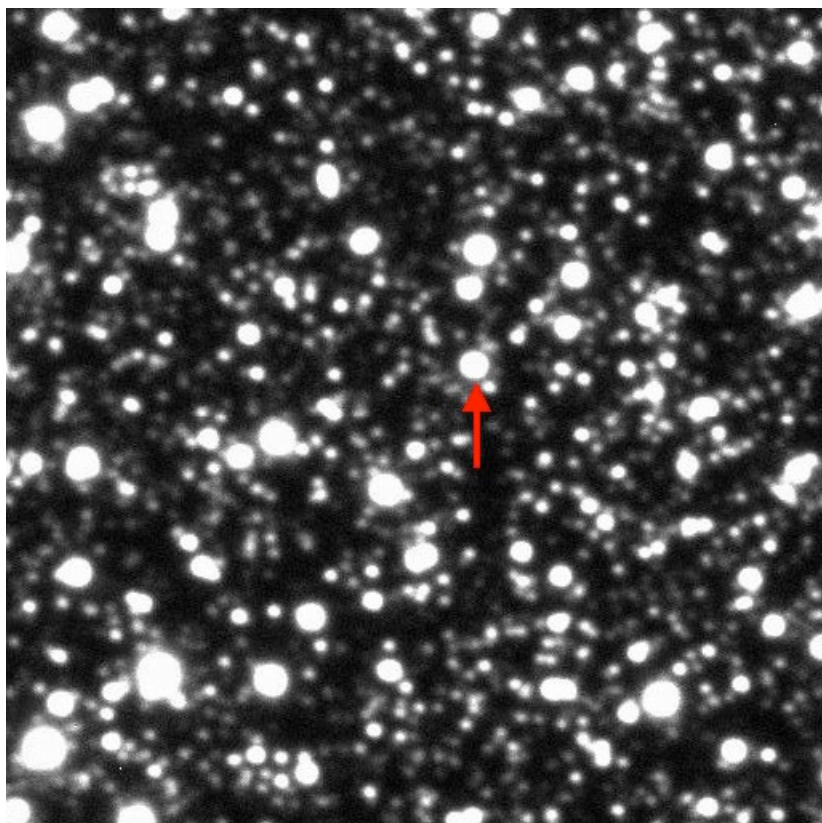


FIG. 2.— The field of view for OGLE-TR-56, as observed on 2008 May 14 with MagIC-e2v on the 6.5 m Baade telescope. Field of view is $38'' \times 38''$, with north up and east to the left.

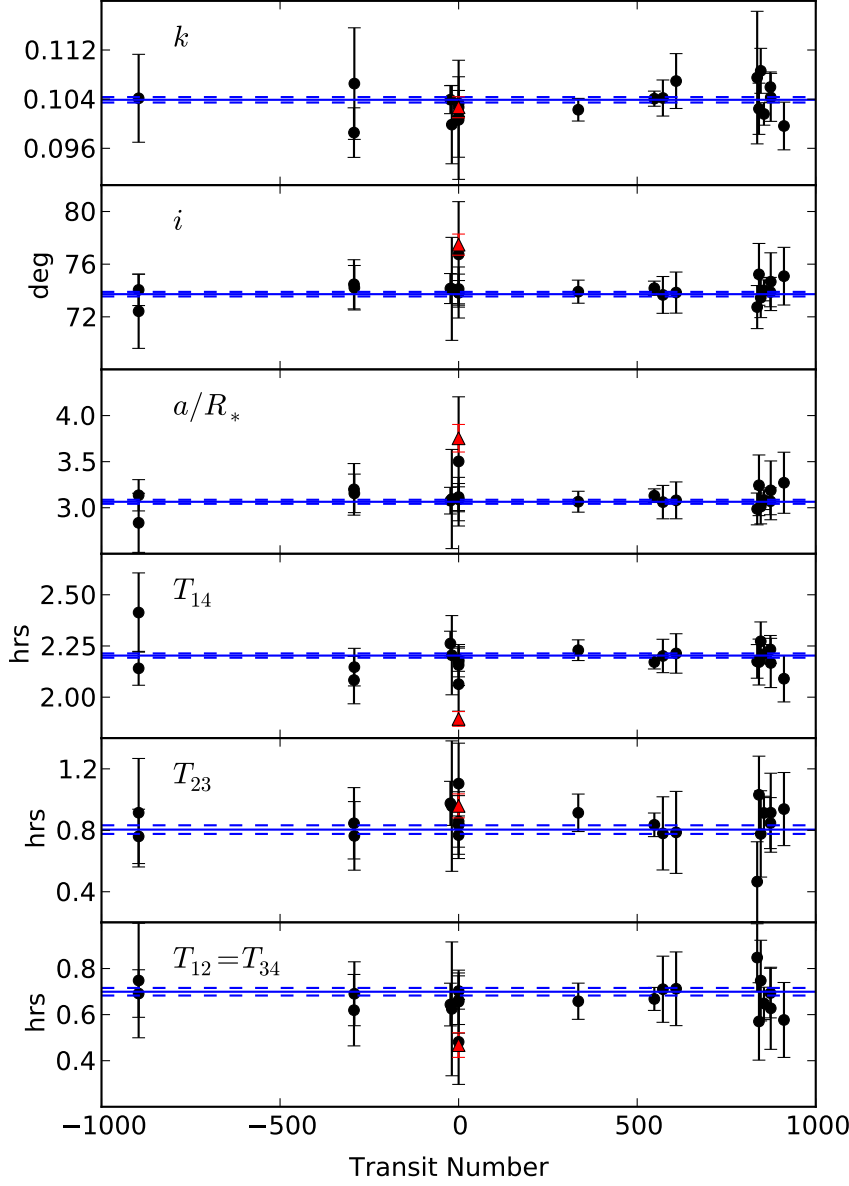


FIG. 3.— Parameter variation of individual transits of OGLE-TR-56b. Data from the individual MCMC fits (Table 5) is shown for the inclination (i), semimajor axis (a/R_*), planet-star radius ratio (k), total transit duration (T_{14}), full transit duration (T_{23}), and ingress/egress duration, assuming a circular orbit ($T_{12} = T_{34}$). Note that all errors have been scaled upward based on the factor calculated from residual permutation. For comparison, the value derived from the joint MCMC fit is plotted as a solid blue lines with dashed $\pm 1\sigma$ errors. We highlight our independent fit to the light curve published by Pont et al. (2007) in red to illustrate that it is markedly discrepant for all parameters except the radius ratio.

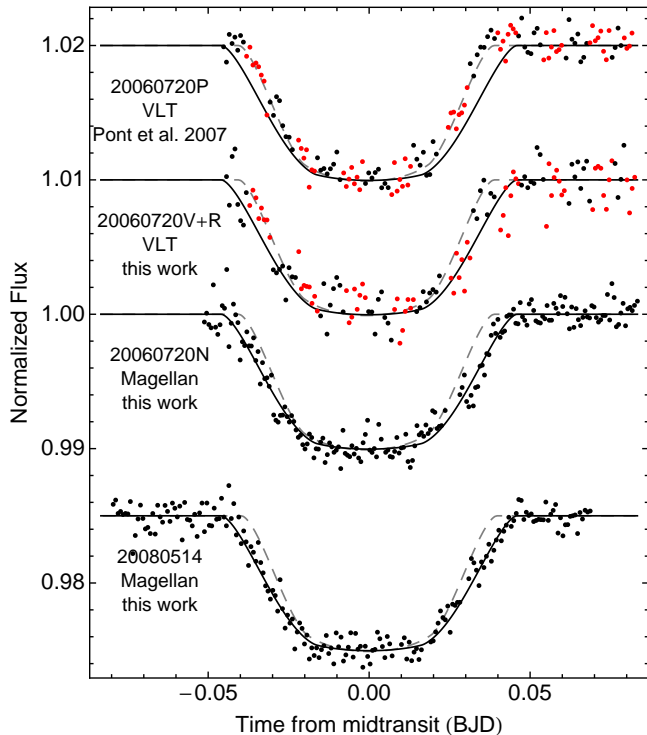


FIG. 4.— Three light curves of the transit on 2006 July 20, observed independently by two instruments, with a fourth curve on a different night for comparison. Data has not been binned. Top curve: original image-subtraction photometry for transit 20060720P observed with FORS1 on the VLT by Pont et al. (2007), with R -band data in red and V -band data in black. Second curve: the same VLT transit, redone with aperture photometry for this work. Third curve: independent observation of the same transit with no filter, 20060720N, using POETS on Magellan (discussed in § 2.1). The bottom curve is a different transit, 20080514, to illustrate the agreement of all but the top curve (20060720P) with the other transits presented in this work. Two models are shown in each plot: a gray dashed line for the best fit to the photometry by Pont et al. (2007) (refit for this work), and a black solid line showing the best joint-fit to all 23 new light curves.

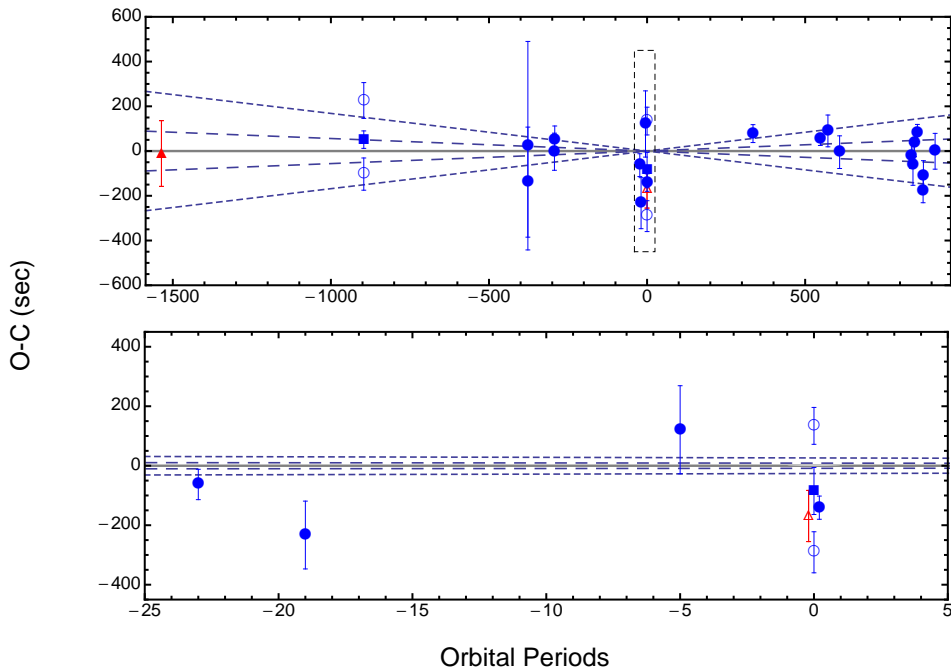


FIG. 5.— Observed minus calculated midtimes for OGLE-TR-56b. Timing residuals using the new ephemeris (Equation 1). Solid symbols mark transits that were used to calculate the ephemeris. The solid red triangle at -1536 is the OGLE midtime, while the open red triangle at 0 is our fit to the photometry from Pont et al. (2007). The two solid blue squares at -896 and 0 represent independent fits to combined-filter light curves, which were used in place of the pair of open circles at those same values, representing each individual filter curve. See § 4 for more details. The bottom panel shows a zoomed-in view of the region around 0 . The solid line shows the expected time of transit, while the dashed lines represent the 1σ and 3σ errors on the calculated orbital period, indicating the slopes that result for a mis-determined period. Notice that the 1σ and 3σ error lines converge around the zero epoch and therefore appear practically indistinguishable in the lower plot.